ISSN 1063-7761, Journal of Experimental and Theoretical Physics, 2013, Vol. 117, No. 1, pp. 21–31. © Pleiades Publishing, Inc., 2013.
Original Russian Text © T.V. Konstantinova, P.N. Melent'ev, A.E. Afanas'ev, A.A. Kuzin, P.A. Starikov, A.S. Baturin, A.V. Tausenev, A.V. Konyashchenko, V.I. Balykin, 2013, published in Zhurnal Eksperimental'noi i Teoreticheskoi Fiziki, 2013, Vol. 144, No. 1, pp. 27–40.

ATOMS, MOLECULES, OPTICS

A Nanohole in a Thin Metal Film as an Efficient Nonlinear Optical Element

T. V. Konstantinova[a], P. N. Melent'ev[a], A. E. Afanas'ev[a], A. A. Kuzin[b], P. A. Starikov[b], A. S. Baturin[b], A. V. Tausenev[c], A. V. Konyashchenko[c], and V. I. Balykin[a,*]

[a] *Institute of Spectroscopy, Russian Academy of Sciences, Troitsk, Moscow oblast, 142190 Russia*
[b] *Moscow Institute of Physics and Technology, Dolgoprudnyi, Moscow oblast, 141700 Russia*
[c] *OOO Avesta-proekt, Troitsk, Moscow oblast, 142190 Russia*
**e-mail: balykin@isan.tyroitsk.ru*

Received November 15, 2012

Abstract—The nonlinear optical properties of single nanoholes and nanoslits fabricated in gold and aluminum nanofilms are studied by third harmonic generation (THG). It is shown that the extremely high third-order optical susceptibility of aluminum and the presence of strong plasmon resonance of a single nanohole in an aluminum film make possible an efficient nanolocalized radiation source at the third harmonic frequency. The THG efficiency for a single nanohole in a thin metal film can be close to unity for an exciting laser radiation intensity on the order of 10^{13} W/cm^2.

DOI: 10.1134/S1063776113080165

1. INTRODUCTIOIN

The study of nonlinear photoprocesses is an important direction in nanooptics and nanoplasmonics [1–4]. Nonlinear photoprocesses in nanoplasmonics are based on three main factors: (i) the possibility of concentrating an electromagnetic energy at the nanometer scale with the help of surface plasmons, resulting in an increase in the local field and, therefore, enhancement of nonlinear effects, (ii) ultrashort relaxation times in the range from 0.1 to 10 fs inherent in metals, and (iii) the possibility of optical excitation of nanostructures by ultrashort femtosecond laser pulses.

By now a variety of nonlinear photoprocesses in nanoplasmonics have been studied, such as second harmonic generation in metal nanostructures [5–10], four-wave mixing on metal surfaces [11], ultrafast optical modulation based on third-order nonlinearity [12–14], and high harmonic generation [15, 16].

Third harmonic generation (THG) is the simplest nonlinear effect, which is allowed in all media and is independent of the symmetry of nanostructures. The nonlinear susceptibility of a metal is determined by free electrons, and the THG physics in metals consists in the displacement of the electron cloud outside the ion core during oscillations caused by the electromagnetic field. The resulting returning force ceases to linearly depend on the displacement of the center of masses of the electron cloud from its equilibrium position and contains nonlinear terms, beginning from the third-order term in the displacement. Such a collective motion of electrons near the surface of nanostructures is responsible for THG [17].

As was shown in [18], an increase in the THG efficiency can be expected with increasing excitation intensity at the fundamental frequency. For radiation field intensity on the order of 10^{16} W/cm^2, the electric field amplitude at the third harmonic frequency can be already on the order of the excitation field amplitude. We will show below that thermal effects prevent the use of such high field intensities for nanoparticles.

The most important THG parameters are (i) the THG efficiency (the power ratio of the third harmonic and exciting radiation and (ii) the THG efficiency per unit mass of a material. In experiments [19], THG was observed in gold nanoparticles using relatively weak exciting laser radiation (10^{10}–10^{11} W/cm^2). To increase the THG efficiency, excitation was performed at a frequency equal to one-third the Mie resonance frequency for nanoparticles, i.e., resonantly with the third harmonic frequency. Nevertheless, the THG efficiency for nanoparticles was low.

An example of nanoparticles in which efficient nonlinear optical conversion can be obtained is optical antennas [1]. It was recently shown [20] that nanoantennas can be efficient nonlinear radiation sources. One of the motivations in optical studies with nanoparticles (in the given case, with nanoantennas) is the possibility of using them to construct a nanosized radiation source. However, nanoparticles as radiation sources have two significant disadvantages. First, exciting radiation produces an intense background and, second, nanostructures are destroyed at high incident radiation powers. The restriction on the exciting radiation power leads to a restriction on the THG efficiency. A nanoobject that can generate the

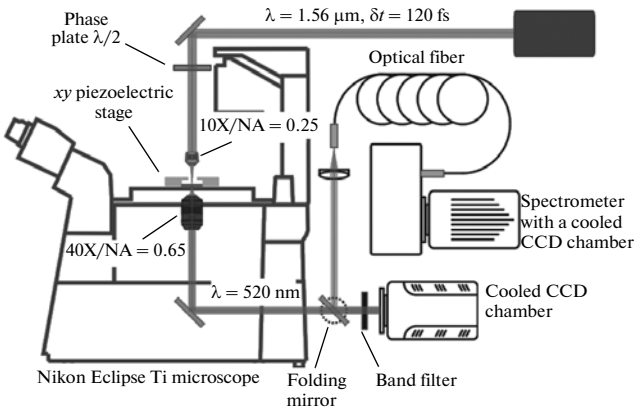

Fig. 1. Scheme of the experimental setup for studying third harmonic generation in single nanoholes.

third harmonic and at the same time have none of these disadvantages is a nanohole in a metal film, which is what we study here

We present the results of THG studies with individual nanoobjects in the form of circular holes and slits made in gold and aluminum films. The influence of the film material and hole geometry on the THG efficiency is investigated. It is shown that the exciting radiation intensity is limited by the melting of nanostructures. The possibility of constructing a nanolocalized radiation source emitting at the third harmonic frequency and devoid of background exciting laser radiation is shown.

The paper is organized as follows. In Section 2, we describe our experimental setup and methods used in studies and also present the main characteristics of samples with nanoholes. In Section 3, the results of THG studies in thin gold and aluminum films are presented. In Sections 4 and 5, THG studies with circular nanoholes and nanoslits are described, respectively. In Section 6, we compare the THG efficiency in gold and aluminum for developing an intense nanolocalized radiation source.

2. EXPERIMENTAL

The scheme of our experimental setup is shown in Fig. 1. The third harmonic was excited by 120-fs, 1560-nm, 15-mW pulses from a femtosecond laser [21] with a pulse repetition rate of 70 MHz. The third harmonic generation was measured with an inverted Nikon Eclipse Ti/U microscope. Laser radiation, focused with a 10X, NA = 0.25 objective into a spot 4.3 μm in diameter in the sample plane, was directed perpendicular to the surface of a film with nanoholes (deviation from the vertical was less than 1°). The peak radiation intensity on a sample was on the order of 1.1×10^{10} W/cm^2. The polarization of incident radiation was controlled with a zero-order λ/2 phase plate for the light wavelength λ = 1560 nm placed in front of a focusing objective. The third harmonic signal was collected with a 40X, NA = 0.65 objective. Exciting radiation was suppressed by means of interference and color filters. Fundamental radiation was additionally suppressed due to chromatic aberration of the objective, which is considerable because of the large difference between the radiation wavelengths at the fundamental frequency and third harmonic frequency. The use of filters and chromatic aberration provided suppression of the fundamental signal by more than 13 orders of magnitude. The spatial distribution of radiation from nanoobjects was studied with a cooled two-dimensional avalanche electron multiplication CCD camera (Princeton Instruments, Photon-MAX). The emission spectrum was recorded with a spectrometer equipped with a cooled CCD array (Princeton Instruments, NTE/CCD-1340/100). Radiation at the input of the spectrometer was spatially filtered with an aperture 40 μm in diameter to reduce the contribution of the parasitic background signal to the spectrum of recorded radiation. The setup was mounted on a vibration isolation table to eliminate the influence of mechanical perturbations.

The THG efficiency depends on the radiation intensity cubed at the excitation frequency. Therefore, in experiments we carefully controlled the position and size of an exciting radiation spot with respect to the position of a nanohole for which THG was studied. For this purpose, the nanohole was placed under focused laser radiation by means of a dual-axis feedback translation stage (CAP201XY, Piezo Jiena) providing durable control of the spatial position of the nanohole with an accuracy about 10 nm. The size of the laser radiation spot on a sample was measured by scanning a nanohole 100 nm in diameter in the sample plane and detecting radiation transmitted through it.

To perform absolute measurements of the third harmonic power, the CCD camera of the microscope was calibrated. For this purpose, 1.56-μm laser radiation was directed into a $LiNbO_3$ nonlinear crystal with

Excitation radiation intensities at 1560 nm used in experiments, third harmonic radiation intensities measured for 50-nm gold and aluminum films, and third-order optical nonlinear susceptibilities calculated from these data

Film material	Exciting radiation peak intensity, W/m^2	Third harmonic radiation peak intensity, W/m^2	$\chi^{(3)}$, m^2/V^2
Au (50 nm)	1.12×10^{14}	3.3×10^2	$(2.3 \pm 0.7) \times 10^{-20}$
Al (50 nm)	1.12×10^{14}	4.1×10^3	$(2.6 \pm 0.8) \times 10^{-17}$

a periodic domain structure to obtain THG. Then, this radiation was coupled to the microscope and focused with a 10X, NA = 0.25 objective; it illuminated a nanohole 400 nm in diameter made in a 100-nm-thick aluminum film. Radiation at the fundamental frequency, second, and fourth harmonics (generated in the nonlinear crystal) was suppressed with optical filters. Radiation transmitted through the nanohole was collected with a 40X, NA = 0.65 objective and recorded with the CCD camera. The signal measured with the CCD camera was calibrated using a commercial power meter.

THG was studied in nanoholes made in 50-nm-thick gold and aluminum films. The film thickness affects the THG efficiency in two ways. A small thickness reduces the attenuation of radiation in the nanohole channel, which, as will be shown below, is important for obtaining high THG efficiency in a nanohole. On the other hand, Fabry–Perot resonances can appear for a certain film thickness, which are produced due to reflection of radiation inside the film from the metal/dielectric interface and change the efficiency of the corresponding nonlinear processes [22, 23].

Nanoholes and nanoslits were fabricated in aluminum and gold films a few nanometers thick. These metal films were prepared on the surface of ultrathin (40-nm-thick) SiO_2 membranes [24]. The surface of these membranes has an extremely low roughness (<1.5 Å), which in turn allowed preparation of high-quality metal films on the side adjacent to the membrane. The high quality of the metal surface minimized the contribution of intense luminescence (parasitic for our measurements) [25] inherent in rough metal surfaces [26]. For this purpose, the smooth side of films was turned to the exciting radiation in all measurements.

Gold films were prepared by thermal evaporation at 1240°C in a vacuum of 1×10^{-6} Torr. Aluminum films were prepared by electron-beam target evaporation in a vacuum of 2×10^{-6} Torr. The thickness of films measured with an atomic-force microscope was 50 ± 5 nm. Samples were prepared in a class 100 cleanroom, while optical measurements were performed in a class 1000 cleanroom.

We studied THG in circular nanoholes and nanoslits. The diameter of circular holes was varied from 50 to 560 nm. Nanoslits were made with different length-to-width ratios; however, the area of the open surface of a nanoslit was the same and equal to that of a nanohole. This allows us to compare the THG efficiencies for nanoholes and nanoslits and determine the influence of the hole geometry for a fixed area of its open surface.

Nanoholes were fabricated using a 30-keV Ga^+ ion beam (FEI Quanta 3D) focused to a spot ~10 nm in diameter. The microscopy of nanoholes was performed in a JEOL JSM-7001F electron microscope with a resolution of 5 nm at relatively low beam energies (about 5 keV). A low energy of the electron beam minimized the parasitic process of carbon deposition on the surface of metal films, which accompanies the electron microscopy of metal surfaces.

Figure 2 shows images of typical samples with nanoholes (Fig. 2a) and nanoslits (Fig. 2b). To avoid the influence of collective plasmon effects, the distance between nanoholes was set at 5 μm. This distance also exceeded the diameter of a laser spot at the fundamental frequency. Nanoholes were arranged in sequence and each of them could be identified and studied separately.

3. THIRD HARMONIC GENERATION IN THIN Au AND Al FILMS

To study how the properties of the material of films (Al and Au) in which nanoobjects (nanoholes and nanoslits) were made affected the nonlinear properties of these objects, we investigated the nonlinear properties of the materials themselves.

Polarization induced in a medium by a field $E(t)$ is described by the expression [27, p. 2]

$$P(t) = \varepsilon_0(\chi^{(1)}E(t) + \chi^{(2)}E^2(t) + \chi^{(3)}E^3(t) + \ldots), \quad (1)$$

where $\chi^{(i)}$ is the nonlinear susceptibility on the ith order. In the general case, the vector nature of the field $E(t)$ should be taken into account; therefore, the first-, second-, and third-order nonlinear susceptibilities are second-, third-, and fourth-rank tensors, respectively. Third harmonic generation is determined by the nonlinear polarization of the medium $P^{(3)}(t) = \varepsilon_0\chi^{(3)}E^3(t)$, which in the case of excitation of the medium by a monochromatic wave $E(t) = E_0\cos(\omega t)$ is described by the expression

$$P^{(3)}(t) = \frac{1}{4}\varepsilon_0\chi^{(3)}E_0^3\cos(3\omega t) + \frac{3}{4}\varepsilon_0\chi^{(3)}E_0^3\cos(\omega t). \quad (2)$$

Expression (2) gives the response of the system to the field at frequency ω and describes generation at frequency 3ω. The THG efficiency is determined by the third-order nonlinearity $\chi^{(3)}$:

$$\chi^{(3)}(\omega) = \frac{\chi^{(1)}(3\omega)E(3\omega)}{E^3(\omega)}. \quad (3)$$

The thickness of films used in experiments is considerably smaller than $\lambda/4\pi$; therefore, the contribution from the dielectric/metal interface to the nonlinear susceptibility dominates over that from the film volume [27]. In this approximation, we can assume that the induced nonlinear dipole moment is localized in a metal near the metal/dielectric interface. In this case, the third-order nonlinearity $\chi^{(3)}$ can be determined from (3) using radiation intensities $I(\omega)$ and $I(3\omega)$ measured at the fundamental and third-harmonic frequencies, respectively. The fields at the fun-

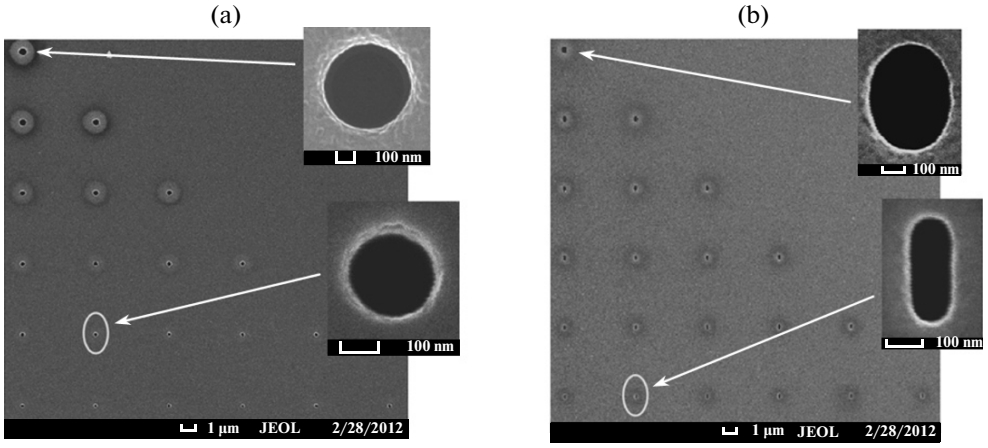

Fig. 2. Scanning electron microscope images of nanoholes in a 50-nm thick Al film: (a) circular nanoholes and (b) nanoslits. The insets show the magnified images of nanoholes.

damental and third-harmonic frequencies in (3) are determined from measurements using the expressions

$$E(\omega) = \left|\frac{2}{n(\omega)+1}\right|\sqrt{\frac{2I(\omega)}{\varepsilon_0 c}}, \quad (4)$$

$$E(3\omega) = \left|\frac{n(3\omega)+1}{2n(3\omega)}\right|\sqrt{\frac{2I(3\omega)}{\varepsilon_0 c}} \times \exp\left(\frac{\alpha(3\omega)}{2}\delta h\right), \quad (5)$$

respectively, where $n(\omega)$ is the complex refractive index of a metal film, δh is the film thickness, and $\alpha(3\omega)$ is the attenuation coefficient of radiation at frequency 3ω in a metal film ($\alpha_{Au}(520\text{ nm}) = 0.047\text{ nm}^{-1}$, $\alpha_{Al}(520\text{ nm}) = 0.15\text{ nm}^{-1}$). The factors at square roots in (4) and (5) are Fresnel amplitude transmission coefficients taking into account the field attenuation in a metal.

The nonlinear properties of Al and Au were studied by focusing the exciting laser radiation on the surface of metal films. Third harmonic generation produced in these experiments was detected with a CCD array. The insets to Fig. 3 show the corresponding optical two-dimensional images of nanoholes (at the third-harmonic wavelength). Note that because of the cubic dependence of the third-harmonic intensity on the fundamental radiation intensity, the third-harmonic radiation is recorded on a CCD array in the form of a spot 2.5 μm in diameter, which is $\sqrt{3}$ times smaller than the diameter of the fundamental radiation spot.

Figure 3 shows the third-harmonic spectra measured in 50-nm-thick Au and Al films for the same exciting radiation intensity (the films had no nanoholes). One can see from this figure that the third harmonic intensity in the Al film is approximately 12 times higher than that in the Au film. Figure 3 also shows the transmission spectra of the Au and Al films used in experiments, which were calculated from data presented in [28, 29]. One can see from the figure that the transmission of the Au film at a wavelength of 520 nm exceeds that of the Al film by a factor of 700! Thus, our measurements show the THG efficiency in aluminum considerably, by a few orders of magnitude, exceeds this efficiency in gold. Using the numerical values of the linear susceptibility $\chi^{(1)}(3\omega) = -4.17 + 3.2i$ for Au [28] and $\chi^{(1)}(3\omega) = -39.2 + 10.9i$ for Al [29], we obtain the corresponding nonlinear susceptibilities $\chi^{(3)}_{Au} = (2.3 \pm 0.7) \times 10^{-20}\text{ m}^2/\text{V}^2$ and $\chi^{(3)}_{Al} = (2.6 \pm 0.8) \times 10^{-17}\text{ m}^2/\text{V}^2$. The temporal shape of a laser pulse at the fundamental frequency was approximated in calculations by a Gaussian with a pulse duration of 120 fs and at the third harmonic frequency by a Gaussian with the pulse duration of $120/\sqrt{3}$ fs. The experimental data used in calculations are presented in table.

As far as we know, these are the first measurements of third-order nonlinearities for gold and aluminum upon excitation at 1560 nm. Theoretical calculations [30] performed for excitation at 1.06 μm predict a value of the third-order susceptibility for aluminum that is 40 times higher than that for gold. The ratio of nonlinear susceptibilities measured at a wavelength of 1.56 μm in our paper is about 10^3. Such a strong difference between the nonlinear properties of gold and aluminum can be explained by the difference between the physical and optical properties of the two metals: (i) the size of nanocrystals in the polycrystalline structure of Al and Au films is different [31], being ~20 nm for gold and ~80 nm for aluminum; (ii) the electronic energy diagrams are different, and the corresponding interband transitions have different frequencies [32].

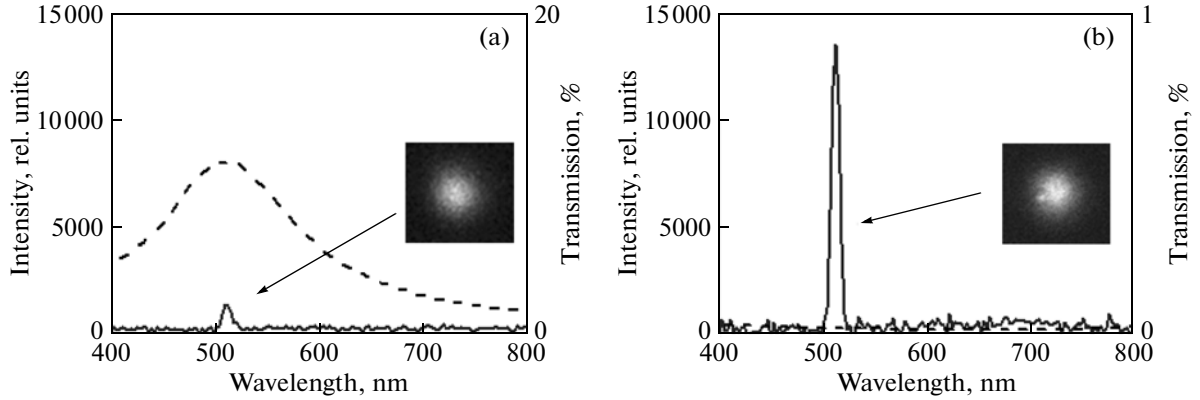

Fig. 3. Emission spectra (solid curves) of (a) Au and Al (b) films irradiated by femtosecond laser pulses at 1560 nm. The dashed curves are transmission spectra calculated for these films. The inset show two-dimensional optical images of nanoholes.

4. THIRD HARMONIC GENERATION IN NANOHOLES IN AU AND AL FILMS

The presence of plasmon resonances in metal nanostructures considerably increases the THG efficiency compared to that in a metal film due to the local increase in the field amplitude. It was shown in [33] that the maximum THG efficiency was achieved in the presence of two simultaneous resonances: at the excitation and third harmonic frequencies.

The influence of plasmon resonances on THG in a large group of nanoholes in a gold film was experimentally demonstrated in [34]. The maximum THG efficiency was achieved in resonance with the excitation wavelength. We demonstrated THG in single nanoholes and an increase in the THG efficiency due to a plasmon resonance at the third harmonic wavelength.

For single nanoholes 50–300 nm in diameter made in a gold film, the plasmon resonance lies in the wavelength range from 500 to 550 nm [35]. Upon irradiation of such a nanohole at a wavelength of 1560 nm, the third harmonic frequency coincides with the plasmon resonance frequency in gold. The presence of this resonance leads to an increase in the THG efficiency from a nanohole compared to that from a gold film without holes. For holes (with the same diameter) in an aluminum film, plasmon resonance is located at 200 nm and, therefore the resonance does not appear upon excitation of a nanohole in Al at 1560 nm. As a result, the plasmon mechanism of enhancing the THG efficiency cannot be realized. Figure 4 shows the experimental dependences of the THG efficiency on the diameter of holes made in gold and aluminum films. The THG efficiency was determined from the expression

$$\eta_{THG} = \frac{1}{\kappa}\frac{P_{THG}}{I(\omega)S_{\text{hole}}}, \qquad (6)$$

where $\kappa = 0.24$ is the radiation collection efficiency of an objective, P_{THG} is the detected THG power from a nanohole, $I(\omega)$ is the radiation intensity at the excitation frequency, and S_{hole} is the nanohole area.

The THG signal detected in experiments is the sum of THG from a thin film and a nanohole. The THG power from the film can considerably exceed that from the nanohole because a greater part of exciting radiation is incident on the film. We determined the contribution to THG from the nanohole by processing the nanohole image profile in an optical microscope, which was obtained by recording radiation at the third harmonic wavelength. This approach is based on the presence of a structure in recorded optical images: (i) a relatively broad pedestal formed by THG in a metal film, whose size is determined by the size of an exciting laser radiation spot, and (ii) a diffraction-limited spot formed by THG in a nanohole. The THG power from the nanohole was calculated from the number of photocounts forming the optical image of this diffraction-limited spot. This approach allowed us to determine the THG signal only from the nanohole (Fig. 4).

One can see from Fig. 4 that the THG efficiency for nanoholes in a gold film is more than an order of magnitude higher than that for holes of the same size in an aluminum film. The maximum THG efficiency for a nanohole in a gold film was 8×10^{-10}. It was achieved for a nanohole 150 nm in diameter.

One can see from Fig. 4 that the THG efficiency increases with increasing hole diameter up to ~200 nm. These data contradict THG data obtained for single gold nanoparticles in [20], where it was found that the THG efficiency increased with decreasing volume of nanoparticles due to the increase in the decay time of localized plasmons. The difference of our results from those obtained in [20] can be explained by the dependence of the transmission of nanoholes on their diameter: due to weak transmission of light through nanoholes with small diameters, the detected THG power is low. In addition, Fig. 4 shows that the THG efficiency decreases for nanoholes with diameters exceeding 200 nm. We explain this by tight

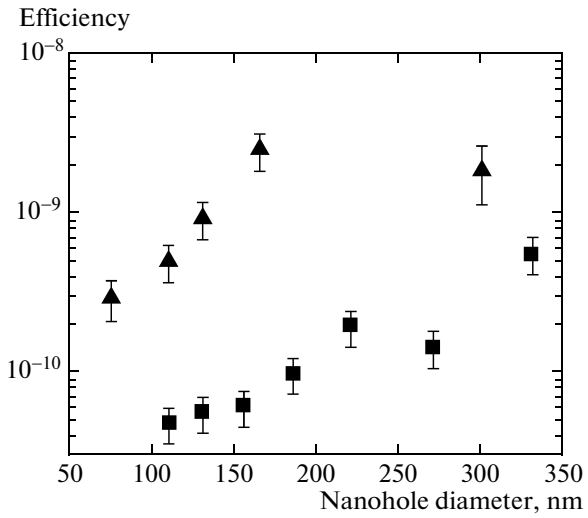

Fig. 4. Third harmonic generation efficiency measured as a function of the hole diameter for single nanoholes in gold (triangles) and aluminum (squares) films.

focusing of exciting laser radiation used in experiments. In the case of large-diameter nanoholes, this reduces the amplitude of the field in which a part of a metal film forming the hole is found.

In concluding this section, we note an interesting fact that the removal of part of the film metal (production of nanoholes) does not reduce the nonlinear response of the metal, but instead enhances it, resulting in a considerable increase in the THG efficiency.

5. THIRD HARMONIC GENERATION IN NANOHOLES IN Au AND Al FILMS

Unlike a nanohole, a nanoslit made in a metal film can have not one but a few resonances because the resonance frequency is determined not only by the optical properties of the film material and its surrounding but also by the nanoslit geometry [36]. It was shown in [37] that, by varying the geometry of a nanostructure, it is possible to obtain resonances in the nanostructure both at the excitation and THG frequencies. This in turn leads to a considerable increase in the THG efficiency. The double resonance can be also used to increase the THG efficiency in nanostructures [33].

Our calculations have shown that the resonance in a nanoslit is obtained at an excitation wavelength of 1.56 μm in an aluminum film when the slit length is ~600 nm. Such a large slit is of no interest for creating a radiation source with nanometer spatial localization. At the same time, plasmon resonance at the THG wavelength (520 nm) can be excited in a nanoslit ~200 nm in length. Such a nanoslit can be already treated as a radiation source with nanometer spatial localization. In this paper, we excited this resonance to increase the THG efficiency in a single nanoslit.

The optimal geometry of a nanoslit was determined using FIT (finite integration technique) computer simulation. We calculated the transmission of a slit for a plane monochromatic wave with a wavelength of 520 nm equal to the THG wavelength and the wave vector directed orthogonally to the slit plane. The incident radiation was polarized perpendicular to the long axis of the slit. Figure 5 shows the transmission of light at wavelengths of 520 and 1560 nm by a nanoslit in a 50-nm-thick aluminum film with a fixed slit width (50 nm) calculated as a function of the slit length. One can see that resonance in transmission at the third harmonic wavelength (520 nm) is achieved for a slit ~170 nm in length. Figure 5 also shows that resonance is absent at the excitation wavelength (1.56 μm) for the chosen nanoslit geometry. Figures 6a and 6b present field distributions upon illumination of a slit by monochromatic radiation at 520 nm for the field polarized along and across the major axis of the slit. One can see that the field is more strongly enhanced when radiation is polarized across the major axis of the slit.

To study THG in nanoholes, we fabricated a set of nanoholes 50 nm × 170 nm in size in a 50-nm-thick aluminum foil. The result of THG measurements in one of these holes is presented in Fig. 6c. One can see that the signal consists of a broad pedestal caused by THG in the metal film and a narrow diffraction-limited peak related to THG in the nanohole. Figure 6c also shows that the THG signal for the polarization of incident radiation corresponding to excitation of a plasmon resonance (polarization along the minor axis of the slit) considerably exceeds the THG signal for orthogonal polarization at which a plasmon resonance is not excited. Similar relations between signals were also obtained for other slits with the same geometry. The THG efficiency was $\sim 10^{-9}$.

We also performed measurements with nanoholes with the same geometry fabricated in a 50-nm/thick gold film. In this case, the THG efficiency was $\sim 7 \times 10^{-10}$.

To study the influence of the film material on the THG efficiency from a nanohole as a nonlinear element, we measured THG for slits with different lengths from 50 to 300 nm in aluminum and gold films. The THG efficiencies measured in these experiments confirmed the resonance properties of a slit 50 nm × 170 nm in size in an aluminum foil.

We also performed comparative measurements of the THG efficiency for a circular nanohole and a nanoslit with the same area for different sizes of holes and different slit geometries. The THG efficiency measured for a circular hole and a nanoslit made in a gold film proved to be approximately the same. However, the situation for an aluminum film is substantially different. The difference between signals from a circular hole and a nanoslit is considerable, the THG signal from the nanoslit being almost 20 times greater than that from the hole. The results of these measurements

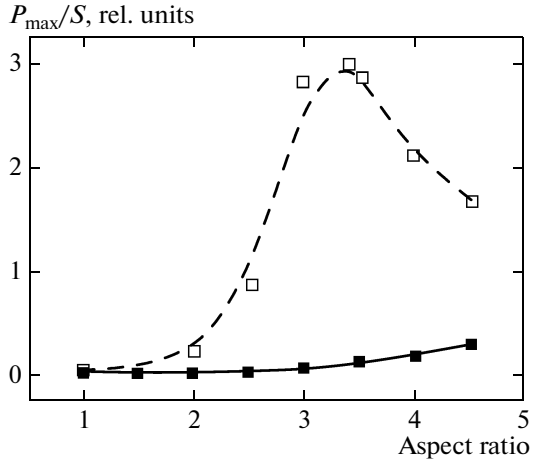

Fig. 5. Transmission P_{max} of light by a single nanoslit at wavelengths 520 nm (dashed curve) and 1560 nm (solid curve) as a function of the ration of slit sides. Transmission is normalized to the nanoslit area S. The nanoslit was made in a 650-nm-thick aluminum film. The slit width was fixed (50 nm), while its length was varied from 50 to 250 nm. The polarization vector of incident radiation is perpendicular to the long axis of the nanoslit.

confirm the contribution of the plasmon resonance to increasing the THG efficiency.

6. COMPARISON OF NONLINEAR PROPERTIES OF GOLD AND ALUMINUM TO CONSTRUCT AN INTENSE NANOLOCALIZED THIRD HARMONIC RADIATION SOURCE

Gold is one of the basic materials for manufacturing elements for nanoplasmonics. However, it was recently shown [38] that aluminum has certain advantages over gold for problems in nanoplasmonics because it possesses stronger nonlinear properties. Studies with aluminum [38] were performed at a wavelength of 780 nm falling into its absorption band. The exciting radiation at 1560 nm used in our paper is strongly detuned from interband electronic transitions in aluminum, which explains the strong nonlinear properties found in aluminum.

The nonlinear properties of gold and aluminum were compared by measuring the THG efficiency for nanoholes of different sizes and shapes (circular holes and slits). As shown above, the THG efficiency depends not only on a material in which nanoobjects were created, but also on their geometry allowing in certain cases the production of plasmon resonances in nanostructures. Figure 7 shows THG efficiencies measured in our work in gold and aluminum nanostructures for the same laser radiation intensity for the following nanoobjects: (i) 50-nm thick nanofilms, (ii) nanoholes 150 nm in diameter, and (iii) nanoslits 50 nm × 170 nm in size. The THG efficiency in thin nanofilms is mainly determined by the optical nonlinear susceptibility of the film material, and, therefore, the THG efficiency in aluminum films proves to be considerably higher than that in gold films.

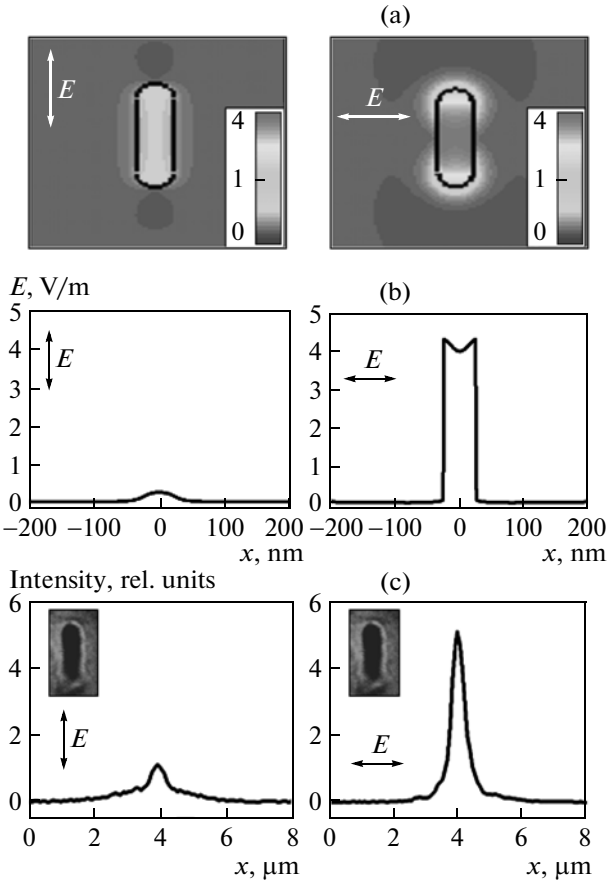

Fig. 6. Third harmonic generation from a nanoslit for different polarizations of exciting radiation. Left: radiation is polarized along the major axis of the nanoslit; right: radiation is polarized perpendicular to this axis. (a) Calculated two-dimensional distribution of the electric-field amplitude amplification on a nanoslit irradiated by a plane monochromatic wave at the third harmonic frequency, (b) corresponding cuts of the calculated distribution of the electric-field amplitude amplification, (c) cuts of the optical image of a nanoslit detected at the third harmonic frequency. The slit 50 nm × 170 nm in size was made in a 50-nm-thick aluminum film.

In nanoholes, plasmon resonance can be excited, which enhances the local field, resulting in turn in a higher THG efficiency. The plasmon resonance frequency in a nanohole depends on the optical properties of the film material and is almost completely independent of the nanohole diameter. It is known that plasmon resonance in nanoholes made in a gold film is observed in the range from 500 to 600 nm. Plasmon resonance for nanoholes in an aluminum film is observed in the UV region; i.e., this resonance is strongly detuned from the THG wavelength studied in our paper. Our measurements of the THG efficiency showed that the nonlinear optical conversion effi-

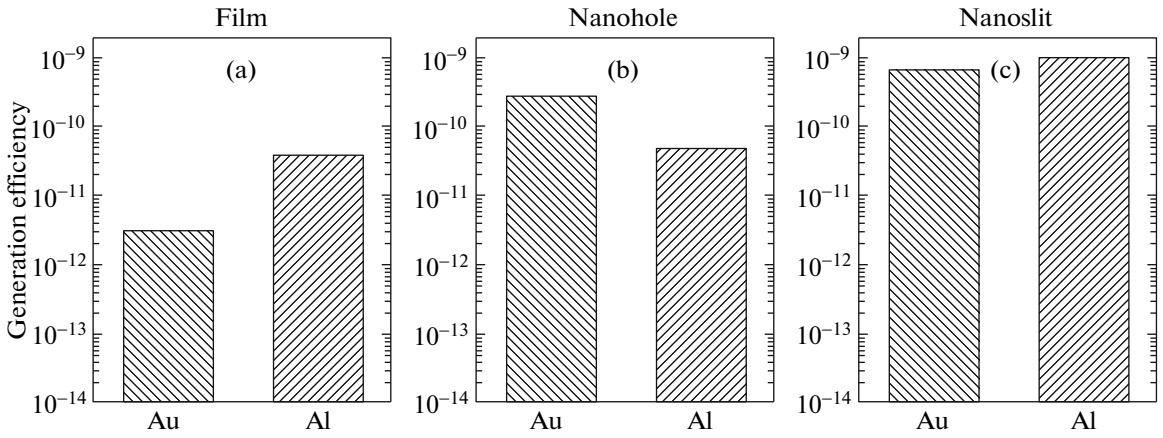

Fig. 7. Comparison of THG efficiencies in gold and aluminum for (a) a 50-nm-thick nanofilm, (b) a nanohole 150 nm in diameter, and (c) a nanoslit 50 nm × 170 nm in size.

ciency for nanoholes in gold films was higher. Thus, the influence of the plasmon resonance in gold nanoholes on the increase in the THG efficiency proved stronger than the influence of the high optical nonlinearity of aluminum.

Plasmon resonance in nanoslits depends not only on the material but also on their geometry because of their high polarizability. In this case, plasmon resonance can be obtained in nanoslits in aluminum at the THG wavelength. Because the optical nonlinear properties of aluminum are stronger than those of gold, the THG efficiency for nanoholes in aluminum is higher, amounting to 10^{-9} (Fig. 7).

A further increase in the THG efficiency can be achieved by increasing the exciting radiation intensity [18] because the induced nonlinear dipole at the triple frequency depends on the incident field amplitude cubed. It was found in [16, 17, 19, 39] that irradiation of gold nanostructures at intensities above 10^{10} W/cm^2 caused their strong heating resulting in melting and a change in their geometry. The heating of nanostructures enhances the scattering of electrons by phonons, reducing the Q factor of plasmon resonances [40]. As the melting point is achieved, nanostructures change their geometrical shape, resulting in a significant change in their optical properties. In particular, this is manifested as a decrease in the local field amplitude, which significantly reduces the efficiency of nonlinear processes. Below, we present the results of our studies on the heating of nanostructures by high-intensity laser radiation, which demonstrate considerable differences between heating temperatures for nanoparticles and nanoholes.

The main objects studied in nanoplasmonics are nanoparticles and complementary nanoholes. According to the Babine principle, the optical properties of nanoparticles and complementary nanoholes are close. Therefore, both nanoparticles and nanoholes can be used for manufacturing nanolocalized radiation sources. Figure 8a shows the temperature distribution in an aluminum nanodisc 100 nm in diameter. This distribution is obtained by the numerical solution of the heat conduction equation taking into account the absorption of the electromagnetic field of exciting radiation with the spatial distribution calculated by the FIT method. Figure 8b shows a similar distribution for nanoholes of the same size made in a 50-nm thick aluminum film. Both structures are illuminated by a plane monochromatic wave at 520 nm with the wave vector directed orthogonal to the nanostructure plane. The radiation intensity is 8×10^{13} W/cm^2. One can see from Fig. 8 that laser irradiation causes the local temperature increase near nanostructures. In this case, the absolute value of the nanodisc temperature exceeds the corresponding that for a nanohole due to a great difference in the heat removal of the material: a nanodisc is surrounded by a poorly heat-conducting dielectric, whereas a metal film with a nanohole provides the efficient heat removal. Note that the radiation wavelength of such aluminum nanostructures is located far away from plasmon resonances.

The temperature distribution in gold nanostructures is substantially different. Figure 9a shows the temperature distribution in gold nanostructures (a nanodisc and a nanohole) identical to nanostructures in Fig. 8. The parameters of exciting radiation are the same as in calculations of the temperature distribution in nanostructures in Fig. 8; however, in this case, laser radiation excites plasmon resonances in gold. One can see from Fig. 9a that a nanodisc is heated up to considerably higher temperatures compared to a nanohole. The presence of strong plasmon resonance in gold at the excitation wavelength leads to large local fields and, as a result, to strong local heating. More efficient heat removal in a nanohole provides lower local temperatures compared to a nanodisc. This has an important consequence: melting of

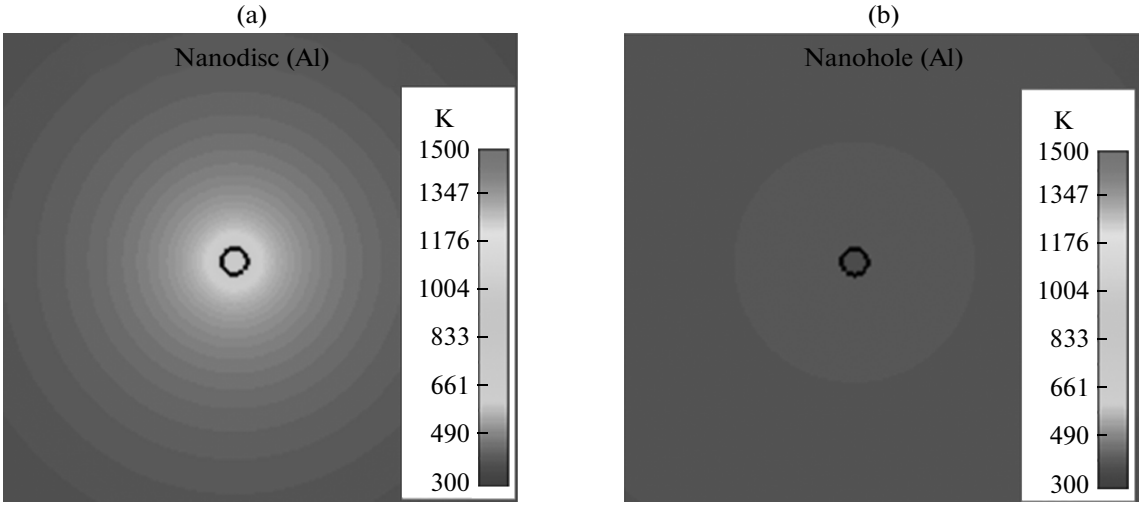

Fig. 8. Spatial temperature distributions calculated for (a) a 50-nm-thick aluminum nanodisc 100 nm in diameter and (b) a nanohole 100 nm in diameter in a 50-nm-thick aluminum film.

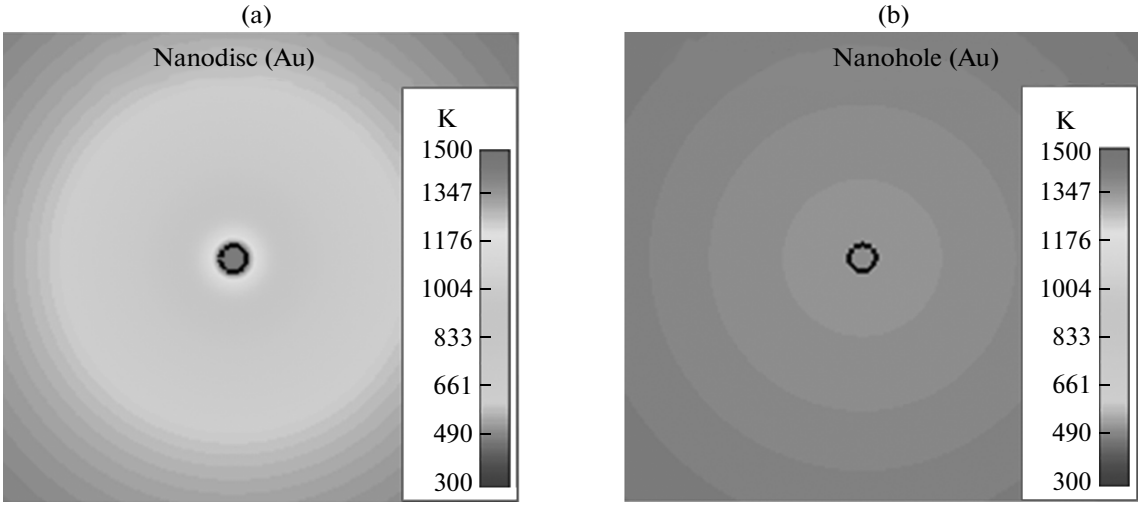

Fig. 9. Spatial temperature distributions calculated for (a) a 50-nm-thick gold nanodisc 100 nm in diameter and (b) a nanohole 100 nm in diameter in a 50-nm-thick gold film.

the disc metal occurs at lower laser radiation intensities compared to nanoholes. This in turn results in higher THG efficiency in nanoholes compared to nanodiscs.

Our calculations of the temperature distribution in nanostructures produced by high-intensity laser radiation showed that an aluminum nanorod 50×170 nm in size begins to melt at laser radiation intensities of about 10^{10} W/cm^2, which is consistent with experimental data [16, 17, 19, 39]. Calculations for a hole in aluminum with the geometry presented in Fig. 6 show that melting is absent at 1.56-μm laser intensities below 10^{13} W/cm^2. This intensity is three orders of magnitude higher than that used in measurements presented in Fig. 6. Our calculations (neglecting an increase in losses in a metal with increasing temperature) based on our measurements show that the THG efficiency in nanoholes with the chosen geometry in aluminum can be close to unity at the laser radiation intensity 10^{13} W/cm^2.

Note that the melting point of a material is important in the production of nanostructures in elements for nanoplasmonics using intense optical fields. For example, the melting point of aluminum ($T = 933$ K) is considerably lower than that of gold ($T = 1337$ K). Due to the lower thermostability of aluminum compared to gold, aluminum nanostructures will be destroyed at lower laser radiation intensities, restricting the efficiency of nonlinear optical processes realized in these nanostructures.

7. CONCLUSIONS

We have demonstrated the operation of a single nanohole in thin gold and aluminum films as an efficient optical nonlinear element. The third harmonic generation of radiation has been obtained in single circular nanoholes and nanoslits. The THG efficiency in nanoholes and thin gold and aluminum films has been studied. The absolute values of the third-order nonlinear susceptibility have been obtained for gold and aluminum at a wavelength of 1560 nm. It has been found that plasmon resonances in circular nanoholes and nanoslits considerably increase the THG efficiency. The third harmonic radiation from such nanostructures forms a nanolocalized radiation source without the background exciting radiation. Note in conclusion that nonlinear optical elements of nanoobjects can be very important in optical nanolithography [16, 41], optical data processing, nanometer optical microscopy, and in nonlinear optical devices [42–44].

ACKNOWLEDGMENTS

This work was supported in part by the Russian Foundation for Basic Research (project nos. 11-02-00804-a, 12-02-00784-a, and 12-02-33073) and the program "Extreme Light Fields" of the Russian Academy of Sciences (RAS). The study was performed using the equipment of CUCs at the Institute of Spectroscopy, RAS, the Moscow Institute of Physics and Technology (project no. 16.552.11.7022), and the Nanotechnology SEC at MIPT. The study was also supported by the Russian FederationMinistry of Education and Science.

REFERENCES

1. L. Novotny and N. van Hulst, Nat. Photonics **5**, 83 (2011).
2. T. Schumacher, K. Kratzer, D. Molnar, M. Hentschel, H. Giessen, and M. Lippitz, Nat. Commun. **2**, 333 (2011).
3. J. A. Schuller, E. S. Barnard, W. Cai, Y. C. Jun, J. S. White, and M. L. Brongersma, Nat. Mater. **9**, 193 (2010).
4. M. Kauranen and A. V. Zayats, Nat. Photonics **6**, 737 (2012).
5. S. Palomba, M. Danckwerts, and L. Novotny, J. Opt. A: Pure Appl. Opt. **11**, 114030 (2009).
6. A. Bouhelier, M. Beversluis, A. Hartschuh, and L. Novotny, Phys. Rev. Lett. **90**, 013903 (2003).
7. M. Labardi, M. Allegrini, M. Zavelani-Rossi, D. Polli, G. Cerullo, S. De Silvestri, and O. Svelto, Opt. Lett. **29**, 62 (2004).
8. M. I. Stockman, D. J. Bergman, C. Anceau, S. Brasselet, and J. Zyss, Phys. Rev. Lett. **92**, 057402 (2004).
9. N. I. Zheludev and V. I. Emelyanov, J. Opt. A: Pure Appl. Opt. **6**, 26 (2004).
10. B. K. Canfield, H. Husu, J. Laukkanen, B. Bai, M. Kuittinen, J. Turunen, and M. Kauranen, Nano Lett. **7**, 1251 (2007).
11. J. Renger, R. Quidant, N. van Hulst, and L. Novotny, Phys. Rev. Lett. **104**, 046803 (2010).
12. T. Utikal, M. I. Stockman, A. P. Heberle, M. Lippitz, and H. Giessen, Phys. Rev. Lett. **104**, 113903 (2010).
13. D. Pacifici, H. J. Lezec, and H. A. Atwater, Nat. Photonics **1**, 402 (2007).
14. K. F. MacDonald, Z. L. Samson, M. I. Stockman, and N. I. Zheludev, Nat. Photonics **3**, 55 (2009).
15. S. Kim, J. H. Jin, Y. J. Kim, I.-Y. Park, Y. Kim, and S.-W. Kim, Nature (London) **453**, 757 (2008).
16. I. Y. Park, S. Kim, J. Choi, D.-H. Lee, Y.-J. Kim, M. F. Kling, M. I. Stockman, and S.-W. Kim, Nat. Photonics **5**, 677 (2011).
17. S. V. Fomichev and W. Becker, Phys. Rev. A: At., Mol., Opt. Phys. **81**, 063201 (2010).
18. S. V. Fomichev, S. V. Popruzhenko, D. F. Zaretsky, and W. Becker, J. Phys. B: At., Mol. Opt. Phys. **36**, 3817 (2003).
19. M. Lippitz, M. Dijk, and M. Orrit, Nano Lett. **5**, 799 (2005).
20. T. Hanke, J. Cesar, V. Knittel, A. Trügler, U. Hohenester, A. Leitenstorfer, and R. Bratschitsch, Nano Lett. **12**, 992 (2012).
21. *Femtosecond laser EFOA-SH* (Avesta, Troitsk, Moscow oblast, 2013). http://www.avesta.ru/pageseng/Femtosecond-Fiber-Laser-EFOA-SH/-172.htm.
22. J. Renger, R. Quidant, and L. Novotny, Opt. Express **19**, 1777 (2011).
23. S. V. Fomichev, D. F. Zaretsky, and W. Becker, Phys. Rev. B: Condens. Matter **79**, 085431 (2009).
24. P. N. Melentiev, A. V. Zablotskiy, D. A. Lapshin, E. P. Sheshin, A. S. Baturin, and V. I. Balykin, Nanotechnology **20**, 235301 (2009).
25. P. N. Melentiev, T. V. Konstantinova, A. E. Afanasiev, A. A. Kuzin, A. S. Baturin, and V. I. Balykin, Opt. Express **20**, 19474 (2012).
26. G. T. Boyd, Z. H. Yu, and Y. R. Shen, Phys. Rev. B: Condens. Matter **33**, 7923 (1986).
27. R. W. Boyd, *Nonlinear Optics* (Academic, London, 2003), p. 127.
28. P. B. Johnson and R. W. Christy, Phys. Rev. B: Solid State **6**, 4370 (1972).
29. A. D. Rakic, Appl. Opt. **34**, 4755 (1995).
30. W. K. Burns and N. Bloembergen, Phys. Rev. B: Solid State **4**, 3437 (1971).
31. G. T. Boyd, Z. H. Yu, and Y. R. Shen, Phys. Rev. B: Condens. Matter **33**, 7923 (1986).
32. E. D. Palik, *Handbook of Optical Constants of Solids* (Academic, Orlando, Florida, United States, 1985), Vol. I.
33. J. F. Reintjes, *Nonlinear Optical Parametric Processes in Liquids and Gases* (Academic, Orlando, Florida, United States, 1984).
34. T. Xu, X. Jiao, and S. Blair, Opt. Express **17**, 23582 (2009).
35. G. Mie, Ann. Phys. (Weinheim) **25**, 377 (1908).

36. E. Popov and N. Bonod, in *Structured Surfaces as Optical Metamaterials*, Ed. by A. A. Maradudin (Cambridge University Press, Cambridge, 2011), p. 1.

37. T. Nakanishi, Y. Tamayama, and M. Kitano, Appl. Phys. Lett. **100**, 044103 (2012).

38. M. Castro-Lopez, D. Brinks, R. Sapienza, and N. F. van Hulst, Nano Lett. **11**, 4674 (2011).

39. S. Link, Z. L. Wang, and M. A. El-Sayed, J. Phys. Chem. B **104**, 7867 (2000).

40. P. N. Melentiev, T. V. Konstantinova, A. E. Afanasiev, A. A. Kuzin, A. S. Baturin, A. V. Tausenev, A. V. Konyaschenko, and V. I. Balykin, Laser Phys. Lett. **10** (7), 075901 (2013). doi:10.1088/1612-2011/10/7/075901

41. V. I. Balykin and P. N. Melentiev, Nanotechnol. Russ. **4** (7–8), 425 (2009)].

42. N. N. Lepeshkin, W. Kim, V. P. Safonov, J. G. Zhu, R. L. Armstrong, C. W. White, R. A. Zuhr, and V. M. Shalaev, J. Nonlinear Opt. Phys. Mater. **8**, 191 (1999).

43. P. N. Melentiev, A. E. Afanasiev, A. A. Kuzin, A. V. Zablotskiy, A. S. Baturin, and V. I. Balykin, Opt. Express **19**, 22743 (2011).

44. P. N. Melentiev, A. E. Afanasiev, A. A. Kuzin, A. V. Zablotskiy, A. S. Baturin, and V. I. Balykin, JETP **115** (2), 185 (2012).

Translated by M. Sapozhnikov